Chapter 2
Magnetic Induction

This chapter covers the physical background of magnetic induction and inductive coupling. The fundamental laws of electromagnetism are briefly reviewed and are applied to a basic inductive element: a piece of conductive wire. The terms self- and mutual inductance are defined and some basic inductor modelling networks are introduced. The final and most substantial part of this chapter is devoted to finite element modelling of coils to calculate their self-inductance, equivalent series resistance and mutual inductance with other coils. Examples illustrate some particular modelling techniques that have proven to be useful for inductive link calculations.

2.1 Maxwell's Equations

All laws of classic electromagnetism are summarised by Maxwell's equations [107]. For a detailed discussion of these laws and their discovery, one is referred to the vast amount of existing handbooks on the topic [35, 57, 58, 68].

2.1.1 Time-Domain, Integral Form

Maxwell's equations are best understood in their integral, time-domain form. The first of Maxwell's equations is Gauss's law. Gauss's law expresses that the surface integral of the electric flux density $\mathbf{D}$ over a closed surface S_C equals the enclosed free charge:

$$\oint_{S_C} \mathbf{D} \cdot \mathbf{dS} = \int_{V_{S_C}} \rho \, \mathrm{d}V \tag{2.1}$$

where ρ is the free charge density and V_{S_C} the volume enclosed by the surface.

Faraday's law states that the line integral of the electric field $\mathbf{E}$ over a closed contour C equals the opposite time-derivative of the enclosed magnetic flux:

$$\oint_C \mathbf{E} \cdot \mathbf{dl} = -\frac{\partial}{\partial t} \int_{S_C} \mathbf{B} \cdot \mathbf{dS} \tag{2.2}$$

where S_C is an arbitrary surface enclosed by C and $\mathbf{B}$ the magnetic flux density.

Maxwell's third equation, being a generalisation of Ampère's law, describes the origin of the magnetic field $\mathbf{H}$. It states that the line integral of $\mathbf{H}$ over a closed contour C is equal to the enclosed conduction current plus the time-derivative of the

B. Lenaerts, R. Puers, *Omnidirectional Inductive Powering for Biomedical Implants*,

enclosed electric flux (= displacement current):

$$\oint_C \mathbf{H} \cdot \mathbf{dl} = \int_{S_C} \mathbf{J} \cdot \mathbf{dS} + \frac{\partial}{\partial t} \int_{S_C} \mathbf{D} \cdot \mathbf{dS} \tag{2.3}$$

where $\mathbf{J}$ is the conduction current density and S_C again is an arbitrary surface enclosed by C.

The fourth of Maxwell's equation states that the magnetic field is divergence free, hence that magnetic field lines always close on themselves:

$$\oint_{S_C} \mathbf{B} \cdot \mathbf{dS} = 0 \tag{2.4}$$

2.1.2 Time-Harmonic, Differential Form

When dealing with sinusoidal signals and linear and time-invariant media, it is much more convenient to work in the frequency domain than in the time domain. The time-harmonic, differential version of Maxwell's equations read [68]:

$$\nabla \cdot \mathbf{D} = \rho \tag{2.5}$$

$$\nabla \times \mathbf{E} = -j\omega\mathbf{B} \tag{2.6}$$

$$\nabla \times \mathbf{H} = \mathbf{J} + j\omega\mathbf{D} \tag{2.7}$$

$$\nabla \cdot \mathbf{B} = 0 \tag{2.8}$$

where $\omega = 2\pi f$ is the angular frequency and a real quantity and f is the frequency. In order not to overload the notation, the same symbols have been used for $\mathbf{D}$, ρ, $\mathbf{E}$, $\mathbf{B}$, $\mathbf{H}$ and $\mathbf{J}$ as in the time domain. All quantities are now function of frequency rather than time however. They have become complex (vector) quantities that represent both amplitude and phase angle of the sinusoid with angular frequency ω. For the remainder of this text, all quantities are assumed to be in their time-harmonic form, unless mentioned otherwise.

All bold quantities in Eqs. (2.5)–(2.8) are complex vector fields in three-dimensional space. All non-bold quantities are scalars. Also the non-bold counterpart of a vector quantity may be encountered, like E for $\mathbf{E}$ for instance. In that case, the quantity is a scalar and only represents the field amplitude and not the field vector as such.

2.1.3 Constitutive Relations and Ohm's Law

The two constitutive relations govern the manner by which $\mathbf{D}$ and $\mathbf{E}$ and $\mathbf{H}$ and $\mathbf{B}$ are related:

$$\mathbf{D} = \epsilon\mathbf{E} = \epsilon_r\epsilon_0\mathbf{E} \tag{2.9}$$

$$\mathbf{B} = \mu\mathbf{H} = \mu_r\mu_0\mathbf{H} \tag{2.10}$$

where ϵ is the electric permittivity and μ is the magnetic permeability. These parameters are often expressed relative to the permittivity ϵ_0 and the permeability μ_0 of free space:

$$\epsilon_0 = 8.854 \times 10^{12}\ \text{F/m} \tag{2.11}$$

$$\mu_0 = 4\pi \times 10^{-7}\ \text{H/m} \tag{2.12}$$

with ϵ_r and μ_r in Eqs. (2.9) and (2.10) being the relative permittivity and relative permeability respectively.

The current density $\mathbf{J}$ in (2.7) only includes conduction currents. The conduction current density $\mathbf{J}$ is given by Ohm's law:

$$\mathbf{J} = \sigma\mathbf{E} \tag{2.13}$$

where σ is the electric conductivity.

In the same way that $\mathbf{J}$ only includes conduction currents, the charge density ρ only includes free charges. Because of preservation of charge, it holds that:

$$\nabla \cdot \mathbf{J} = -j\omega\rho \tag{2.14}$$

This equation is also obtained by taking the divergence of Ampère's law (2.7).

It must be stressed that ϵ, μ and σ in (2.9), (2.10) and (2.13) are macroscopic parameters that link macroscopic field quantities. Their physical basis lies in the microscopic behaviour of atoms and molecules in response to EM fields. These parameters are simple constants only for linear, homogeneous, time-invariant and isotropic media. Note that the time-harmonic formulation of Maxwell's equations already implicitly assumes a linear and time-invariant medium.

The term $j\omega\mathbf{D}$ in Ampère's law (2.7) is the displacement current density. This term is responsible for electromagnetic wave propagation. In the near field, it depends on the relative magnitude of σ and $\omega\epsilon$ if either the conduction current or the displacement current is dominant. In conductive media, the contribution of $j\omega\mathbf{D}$ can normally be neglected.

2.1.4 Magnetic and Electric Potential

The magnetic vector potential $\mathbf{A}$ is defined as a vector field for which applies that [58]:

$$\mathbf{B} = \nabla \times \mathbf{A} \tag{2.15}$$

Since a vector field is not unambiguously defined by its curl only, a divergence $\nabla \cdot \mathbf{A}$ is yet to be chosen. This degree of freedom in the definition of $\mathbf{A}$ is usually exploited

to simplify the equations when solving for **A** in EM field solvers (see Sect. 2.5). For now however, the divergence of **A** is set to zero:

$$\nabla \cdot \mathbf{A} = 0 \tag{2.16}$$

By use of the magnetic vector potential, Faraday's law (2.6) can be rewritten as

$$\nabla \times (\mathbf{E} + j\omega\mathbf{A}) = 0 \tag{2.17}$$

As a rotation-less field can be expressed as the negative gradient $-\nabla V$ of a potential function V, it follows that:

$$\mathbf{E} = -\nabla V - j\omega\mathbf{A} \tag{2.18}$$

$$= \mathbf{E_c} + \mathbf{E_m} \tag{2.19}$$

in which V is the electric potential function.

The electric field is hence split up into components $\mathbf{E_c}$ and $\mathbf{E_m}$. The conservative electric field $\mathbf{E_c}$, fully defined by V, originates from positive and terminates on negative charges. These charges are described by the charge distribution function ρ in Gauss's law (2.5). The other part of the electric field, $\mathbf{E_m}$, is magnetically induced and is divergence free. It does not originate from charge distributions, neither does it terminate on them. $\mathbf{E_m}$ forms self-closing field lines just like the magnetic field does. In this way, physical meaning can be given to **A**, since its negative time derivative is the non-conservative component $\mathbf{E_m}$ of the electric field.

2.1.5 Current and Flux

The macroscopic quantities electric current I and magnetic flux ϕ through a certain surface S_C are obtained by integration of their vector counterparts **J** and **B** over that surface:

$$I = \int_{S_C} \mathbf{J} \cdot \mathbf{dS} \tag{2.20}$$

The surface integration of **B** can be replaced by a line integration of the vector potential **A** through Stokes' theorem [25]:

$$\phi = \int_{S_C} \mathbf{B} \cdot \mathbf{dS} \tag{2.21}$$

$$= \oint_C \mathbf{A} \cdot \mathbf{dC} \tag{2.22}$$

where C is the contour enclosing the surface S_C.

2.2 Conductive Wire

Induction coils used for inductive powering, and practical inductors in general, are all made up out of metal wires or traces. Hence it is instructive to investigate the electromagnetic field configuration in and around a piece of conductive wire. The dimensions of the wire and the coil constructed out of it, are assumed to be much smaller than a wavelength, so that the electromagnetic field changes can be considered immediate over the volume of interest and hence that only the near field hence is important.

Figure 2.1 depicts a piece of conductive wire. A potential difference ΔV is applied between both terminals. This gives rise to an electric field $\mathbf{E_c}$, also indicated on the figure, which is described by the voltage function V through:

$$\mathbf{E_c} = -\nabla V \tag{2.23}$$

$\mathbf{E_c}$ is a conservative vector field that relates to a certain charge density ρ through Gauss's law (2.5). The distribution of these charges over the wire depends on the wire and winding geometry and possibly on the definition of given electric potentials in the direct environment. The charges are schematically indicated with $+$ and $-$ signs for a loop-shaped piece of wire in Fig. 2.1. Note that $\mathbf{E_c}$ may be much stronger in the medium in between terminals, where distances can be shorter, than along the wire. This is especially the case in coil windings where high-potential turns lay next to low-potential turns (in multiple-layer windings for example). These charges are directly responsible for the inter-winding capacitance of a coil (see Sect. 2.4 on inductor models of this chapter).

A voltage drop over a piece of conductive wire gives rise to an electric current through it. The resulting magnetic field $\mathbf{H}$ (Fig. 2.1) is obtained from Ampère's law (2.7). For non-magnetic media, the constitutive relation (2.10) becomes:

$$\mathbf{B} = \mu_0 \mathbf{H} \tag{2.24}$$

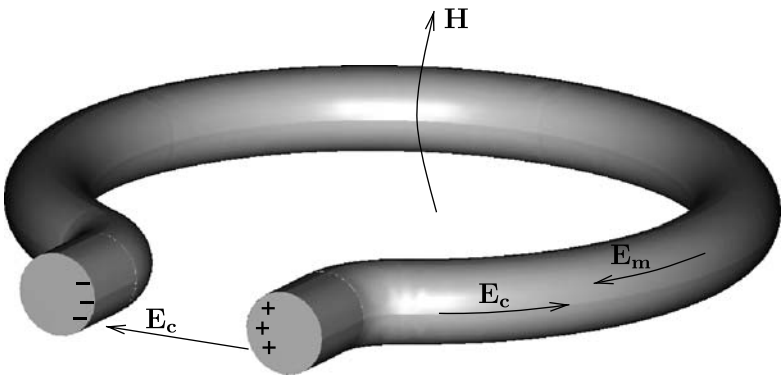

Fig. 2.1 Electric and magnetic field in and around a piece of conductive wire

with μ_0 the permeability of vacuum. Often, ferromagnetic materials are employed in inductors. Although these materials exhibit a non-linear B-H relationship, a linear approximation can still be used for low to moderate field amplitudes. The relative permeability μ_r of ferromagnetic materials ranges from 10^2 to 10^6 [12].

A time-varying magnetic flux density $\mathbf{B}$ gives rise to a non-conservative electric field $\mathbf{E_m}$, according to Faraday's law (2.6). Still considering $\nabla \cdot \mathbf{A} = 0$, $\mathbf{E_m}$ is:

$$\mathbf{E_m} = -j\omega\mathbf{A} \tag{2.25}$$

The $\mathbf{E_m}$ field counteracts the source field $\mathbf{E_c}$, as schematically indicated in Fig. 2.1. This can be easily deducted from the integral, time-domain form of Maxwell's equations (Ampère's law (2.3) and Faraday's law (2.2)). Consequently, the electric current density is restricted, even in an ideal conductor.

While $\mathbf{E_c}$ is more or less homogeneous over the wire cross-section, only varying with the bending radius of the wire, $\mathbf{E_m}$ in general is not. This is because $\mathbf{A}$ is heterogeneous over the wire cross-section. Because neighbouring current distributions affect each other through this $\mathbf{E_m}$ field, the current density in general is heterogeneous over the wire cross-section. This phenomenon is referred to as skin effect when only a single wire cross-section is involved, and as proximity effect when the influence of the current through one wire cross-section on that through another is considered [91, 118, 126].

The current density $\mathbf{J}$ is determined by the total electric field strength:

$$\mathbf{J} = \sigma\,(-j\omega\mathbf{A} - \nabla V) \tag{2.26}$$

Through σ, and the resulting $\mathbf{J}$, the equations for magnetic field (2.7) and electric field (2.6) are coupled. Both equations have to be solved simultaneously in order to find the eventual current distribution and magnetic field. Computational electrodynamics modelling techniques can be used to numerically solve the equations for a given problem [105, 106]. Section 2.5 explains how finite element modelling can be employed to find the magnetic field and current distribution for a given winding geometry.

By integration of the current density $\mathbf{J}$ over the wire cross-section and knowledge of the potential difference ΔV across the wire, the impedance $Z = \frac{\Delta V}{I}$ of that piece of wire can be evaluated. This is illustrated with some examples in Sect. 2.5.

2.3 Inductance

The self-inductance L_1 of a closed circuit C_1 is defined as the ratio of the magnetic flux ϕ_1 it encloses to the electric current I_1 it carries, producing this flux. Hence:

$$\phi_1 = L_1 I_1 \tag{2.27}$$

In the same way does the mutual inductance M_{12} relate the flux ϕ_2 enclosed by a secondary circuit C_2 to the current I_1 in a primary circuit, producing the flux:

$$\phi_2 = M_{12} I_1 \tag{2.28}$$

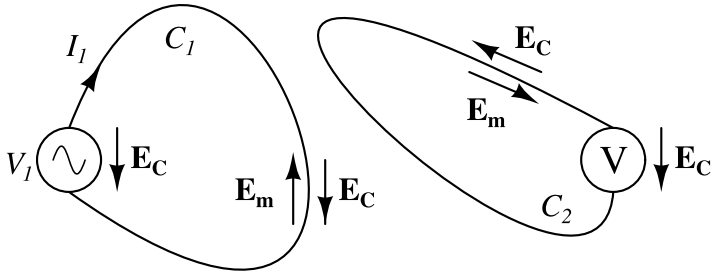

Fig. 2.2 Two closed conductive circuits. *Circuit* C_1 comprises a voltage source, *circuit* C_2 a voltmeter

It can be rigorously proved that $M_{21} = M_{12} = M$. This is done for example by Neumann's equation [59, 112].

Now assume two perfectly conductive, closed circuits C_1 and C_2, both with an infinitesimally small cross-section (Fig. 2.2). In C_1 a voltage source is connected in series, producing a current I_1. In C_2 a voltmeter is incorporated, exhibiting a high impedance that prohibits any current flow. The electric field is split up into $\mathbf{E_c}$ and $\mathbf{E_m}$, in accordance with expression (2.18). Assuming perfect conductors with an infinite conductivity σ, the total electric field is zero both in C_1 and C_2. This is true since otherwise $\mathbf{J}$ would be infinite according to Ohm's law (2.13). Hence, inside the conductive circuits

$$\mathbf{E_m} = -\mathbf{E_c} \tag{2.29}$$

In circuit C_1, $\mathbf{E_c}$ originates from the voltage source terminals, while the $\mathbf{E_m}$ component is magnetically induced. Integration of Faraday's law (2.6) over C_1 yields, by use of Stokes's theorem:

$$\oint_{C_1} \mathbf{E} \cdot \mathbf{dl} = \oint_{C_1} \mathbf{E_m} \cdot \mathbf{dl} = -j\omega\phi_1 \tag{2.30}$$

Since (2.29) applies for a perfect conductor, the produced electromotive force (emf) in (2.30) must equal the source voltage V_1, with only a difference in sign:

$$V_1 = j\omega L_1 I_1 \tag{2.31}$$

This is the equation used in electric circuit theory for an inductive impedance. It can be regarded as a more general definition of inductance. Where (2.27) is limited to closed circuits, (2.31) is not. Though (2.27) has been derived for the case of a closed circuit, it can be used to relate current and voltage between any two nodes of a circuit.

Analogously, in circuit C_2 of Fig. 2.2, the induced emf is:

$$\oint_{C_2} \mathbf{E} \cdot \mathbf{dC} = \oint_{C_2} \mathbf{E_m} \cdot \mathbf{dC} = -j\omega\phi_2 \tag{2.32}$$

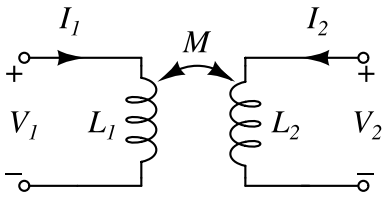

Fig. 2.3 Electric two-port representation of two coupled inductors

Again, because of (2.29), the voltage V_2 across the voltmeter must equal the induced emf with only a difference in sign:

$$V_2 = j\omega M I_1 \tag{2.33}$$

Also this equation is more general than the original definition (2.28), which is limited to closed loops. Through Eq. (2.33), a mutual inductance can be defined between two two-terminal elements, relating the current through one of them with the voltage across the other.

Two magnetically coupled inductors are electrically described by a two-port network (Fig. 2.3). The impedance matrix $\mathbf{Z}$ incorporates both self- and mutual inductances (2.31) and (2.33):

$$\mathbf{V} = \begin{bmatrix} V_1 \\ V_2 \end{bmatrix} = \begin{bmatrix} j\omega L_1 & j\omega M \\ j\omega M & j\omega L_2 \end{bmatrix} \begin{bmatrix} I_1 \\ I_2 \end{bmatrix} = \mathbf{ZI} \tag{2.34}$$

The coupled inductors may be closed circuits or open pieces of wire. In the latter case, the effective L and M values are affected by the current flow to and from that piece of conductor, i.e. the remainder of the circuit. If this contribution is disregarded, one speaks of the partial inductance of that particular piece. Thinking in terms of partial inductance only makes sense in inductance calculations. In real life, current always flows in loops and the magnetic contribution of the complete circuit is measured over each individual piece of conductor.

When a set of K conductor segments are connected in series, the total inductance of that network can be calculated as the sum of the partial inductances L_i of all segment and the mutual inductances M_{ij} from each segment to all others [112]. Indeed, the voltage V across the inductor is the sum of the voltages across the K segments:

$$V = \sum_{i=1}^{K} \sum_{j=1}^{K} j\omega M_{ij} I \tag{2.35}$$

where $M_{ii} = L_i$ and I the current that flows through all K segments. The mutual inductances M_{ij} may have positive or negative values, depending on the polarities of the induced voltages. Hence

$$L = \sum_{i=1}^{K} \sum_{j=1}^{K} M_{ij} \tag{2.36}$$

Consider a loop for example that is cut into two segments with partial inductances L_1 and L_2. The total inductance L can than be written as:

$$L = L_1 + L_2 - 2M \tag{2.37}$$

where the mutual inductance M between both segments is positive. The total inductance hence is smaller than the sum of the partial inductances. This is because the oppositely directed current of one segment counteracts the magnetic field induced by the other segment. The produced emf is in this way restricted in comparison with infinitely far separated segments. When the opposite current directions are separated farther, the enclosed magnetic flux is higher.

2.4 Inductor Models

Perfect inductor models, as expressed by (2.34) will usually be found inadequate to describe the behaviour of real-world coils. More accurate models are obtained by adding a resistor and a capacitor and eventually by breaking up the original inductance into segments.

To start with, an equivalent series resistance (ESR) R is added (Fig. 2.4), comprising all losses associated with the coil. It includes the ohmic losses in the inductor wiring but can be expanded to include losses in surrounding media as well, like ferromagnetic cores or nearby conductive objects.

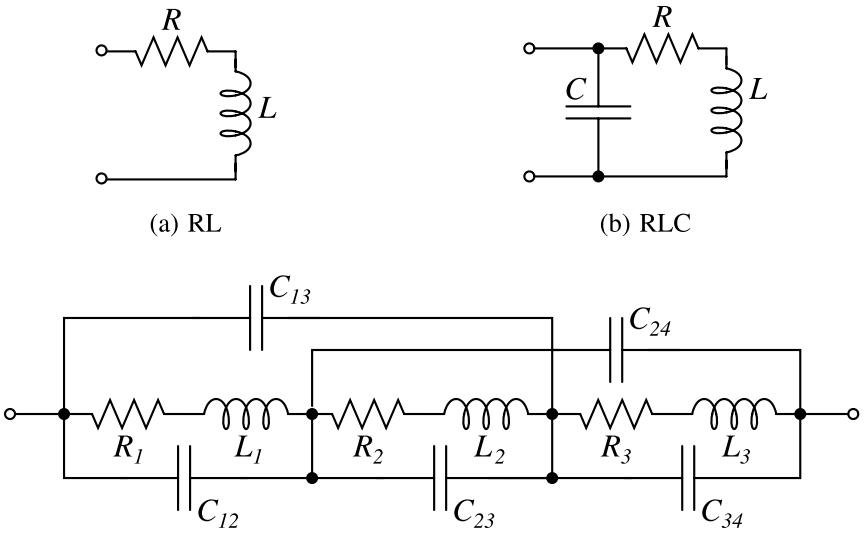

(a) RL (b) RLC

(c) Segmented RLC (three segments)

Fig. 2.4 Some inductor modelling networks

To model self-resonance, a parallel capacitance C is added (Fig. 2.4). As mentioned in Sect. 2.2, the charge density ρ that goes together with the voltage across the inductor, makes a capacitance to be seen between both terminals. The more charge is present, the higher the capacitance is. For a wound inductor, high charge densities arise from:

- a large number of turns,
- short distances between turns,
- high-potential turns laying next to low-potential turns, like in a multiple-layer winding,
- a high-permittivity medium in between turns.

Apart from its permittivity, a dielectric material is also characterised by its dissipative losses. These can be expressed using a complex permittivity $\epsilon = \epsilon' + j\epsilon''$ [69]. The loss tangent $\tan\delta$, which is the inverse of the quality factor Q, of the material is:

$$\tan\delta = \frac{1}{Q} = \frac{\epsilon''}{\epsilon'} = \frac{\sigma}{\omega\epsilon'} \tag{2.38}$$

where σ again is the conductivity, used here as an alternative parameter to model losses in a dielectric material.

The dielectric losses associated with the inter-winding capacitance of a coil may be modelled by an additional series resistance, or can be included in the ESR of the inductor. Usually however, they are negligible compared to the losses associated with the inductance.

More accurate models are obtained by breaking up the inductor into segments, each of them capacitively coupled with all other segments. In this way, models can be constructed that are valid above self-resonance. The segmented coil model in Fig. 2.4 is only one possible example of this approach.

Figure 2.5 shows the different frequency characteristics for the models proposed in Fig. 2.4. Five segments are used for the segmented RLC model. The higher one goes in frequency, the more segments are needed to end up with a valid model. In the limit, for an infinite amount of segments, a continuous RLC distribution is obtained.

An inductor split up into segments can also be considered as a multi-port network, with each node in the circuit constituting a port. Apart from the partial self-inductance of each segment, a mutual inductance is defined with all other segments [112]. This approach may be used to construct a model out of a given coil geometry. To account for skin and proximity effect, each segment is further divided into parallel filaments [74, 111]. From EM theory, a system of equations can be formulated to find all elements of the impedance matrix of the multi-port network. This approach is followed in some inductance calculation routines, like FASTHENRY [74]. The latter one does not include capacitances. Hence, only equivalent RL models can be extracted from the calculated multi-port impedance matrix.

As the coils in an inductive link are normally operated below, or in extremis at self-resonance, RLC models are sufficiently accurate. Well below self-resonance, even a plane RL model is acceptable. The inter-winding capacitance may be absorbed into capacitors connected in parallel with the coil.

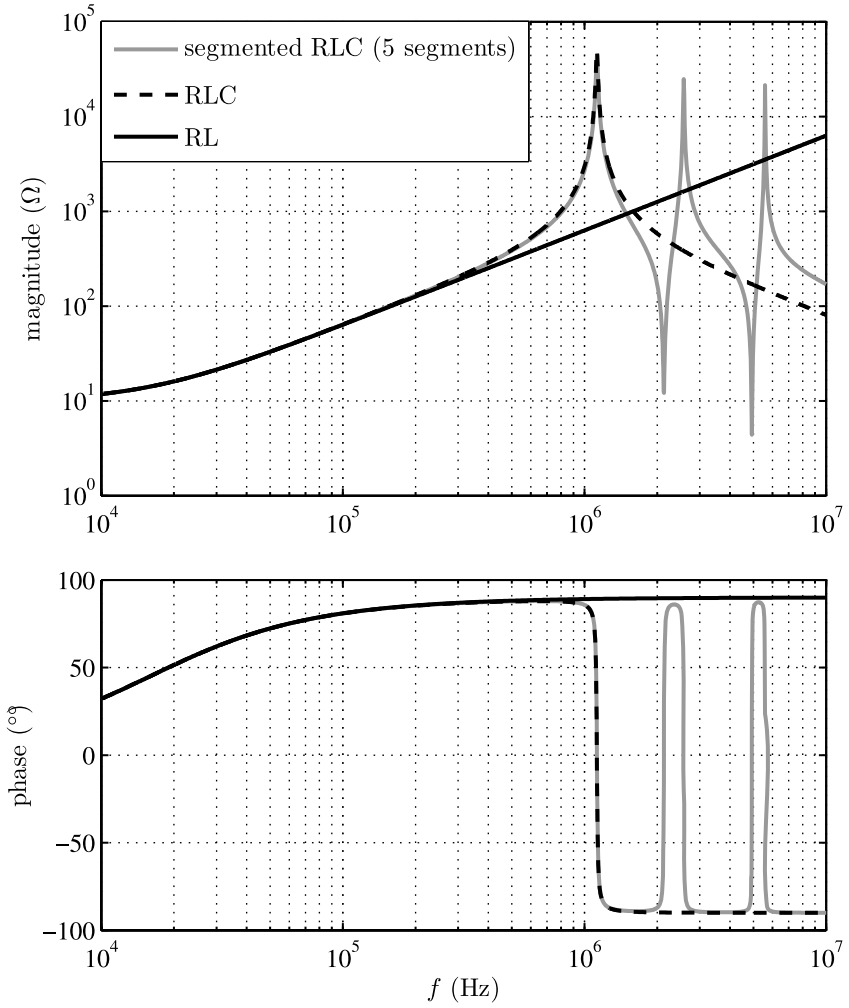

Fig. 2.5 The impedance of some distinct inductor modelling networks vs. frequency f

In general, the inductances and especially the resistances in one-port lumped models are frequency dependent, not because of the influence of parasitic capacitances, but due to the fact that the electric current distribution depends on the frequency. Section 2.5.1 elaborates on this phenomenon, referred to as skin and proximity effect. It can be stated already that the effect on the inductance is minor as long as the wire cross-section is much smaller than the coil dimensions, which is the case for most inductive link applications. This is true because a current redistribution within the wire does not affect the magnetic flux density at longer distances from the wire. The equivalent series resistance on the other hand can change several orders of magnitude with frequency. The R values in Fig. 2.4

therefore have to be specified as a function of frequency in order to be accurate.

2.5 Finite Element Modelling

Maxwell's equations can be numerically solved for a given geometry and electromagnetic source by means of a finite element (FE) package. In the examples further on in this section, COMSOL MULTIPHYSICS has been used [19].

For translating a physical problem into a FE model, the inclusion of an external source current density $\mathbf{J^e}$ can be useful [21]. Maxwell's fourth equation (2.7) then becomes:

$$\nabla \times \mathbf{H} = \sigma \mathbf{E} + j\omega \mathbf{D} + \mathbf{J^e} \tag{2.39}$$

The external current density $\mathbf{J^e}$ stands separate from the conduction current $\sigma \mathbf{E}$. It merely serves as an input for the model.

Using the definition of magnetic and electric potentials (2.15) and (2.18) and the constitutive relations (2.9) and (2.10), one obtains:

$$\nabla \times \left(\mu^{-1} \nabla \times \mathbf{A}\right) + \left(j\omega\sigma - \omega^2 \epsilon\right) \mathbf{A} + (\sigma + j\omega\epsilon) \nabla V = \mathbf{J^e} \tag{2.40}$$

A second equation is obtained by taking the divergence of (2.40):

$$\nabla \cdot \left[\left(j\omega\sigma - \omega^2 \epsilon\right) \mathbf{A} + (\sigma + j\omega\epsilon) \nabla V - \mathbf{J^e}\right] = 0 \tag{2.41}$$

which is in fact the equation of continuity (2.14). Equations (2.40) and (2.41) make out a system of equations that can be solved for the two potentials $\mathbf{A}$ and V. This system can be reduced to one equation by combining V and $\mathbf{A}$ into one vector potential $\tilde{\mathbf{A}}$:

$$\mathbf{E} = -j\omega \mathbf{A} - \nabla V = -j\omega \tilde{\mathbf{A}} \tag{2.42}$$

Note that by this definition $\tilde{\mathbf{A}}$ is no longer divergence free, like $\mathbf{A}$ was, but includes the gradient field $-\frac{j}{\omega} \nabla V$. By use of $\tilde{\mathbf{A}}$, V vanishes from the equations and (2.40) becomes:

$$\nabla \times \left(\mu^{-1} \nabla \times \tilde{\mathbf{A}}\right) + \left(j\omega\sigma - \omega^2 \epsilon\right) \tilde{\mathbf{A}} = \mathbf{J^e} \tag{2.43}$$

If no explicit solution for V is needed, and an external current density $\mathbf{J_e}$ can be applied as input rather than a voltage, working with $\tilde{\mathbf{A}}$ is the preferable option. In that case, only (2.43) is to be solved. In all other cases, Eqs. (2.40) and (2.41) have to be solved simultaneously for $\mathbf{A}$ and V. The field quantities $\mathbf{B}$ and $\mathbf{E}$ are obtained from the solution as in (2.15) and (2.42).

The remainder of this section elaborates on some particular types of FE models that have proven to be useful for inductive link design. For finding out more about the software package itself, and especially about how to construct such models, one is referred to the COMSOL MULTIPHYSICS user manuals [19–21].

2.5.1 Axisymmetric Geometries

Coil windings encompassing circular turns around a common axis can be treated, up to a certain degree of accuracy, as axisymmetric structures. This category includes, but is not limited to, solenoids and spiral coils. An axisymmetric model only has two spatial dimensions: radius r and height z. This implies that there is no variation of the field quantities along the third dimension, φ in cylindrical coordinates (Fig. 2.6). The geometry modelled is a solid of revolution around the z-axis.

In an axisymmetric coil model, current only flows through, and not in, the r-z plane. $\mathbf{J^e}$ as well as $\mathbf{E}$ and $\tilde{\mathbf{A}}$ are orthogonal to the r-z plane and reduce to the scalar variables J^e_φ, E_φ and A_φ. The conservative contribution $-\nabla V$ is zero, since no potential variation is supported along dimension φ. Equation (2.40) thus simplifies to:[1]

$$-\frac{1}{\mu}\nabla^2 A_\varphi + \left(j\omega\sigma - \omega^2\epsilon\right) A_\varphi = J^e_\varphi \tag{2.44}$$

For the solved axisymmetric model, the total current density J_φ equals:

$$J_\varphi = \sigma\left(-j\omega A_\varphi\right) + J^e_\varphi \tag{2.45}$$

The total electric field E_φ hence is:

$$E_\varphi = -j\omega A_\varphi + \frac{J^e_\varphi}{\sigma} \tag{2.46}$$

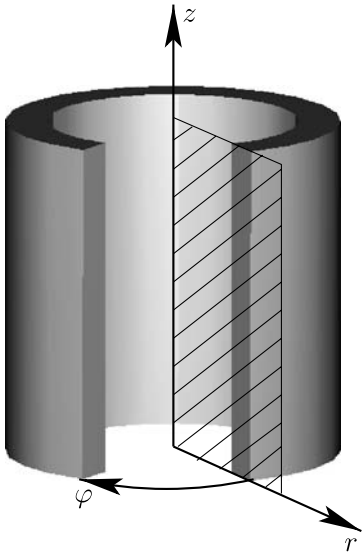

Fig. 2.6 Cylindrical coordinates r, z and φ. An axisymmetric geometry can be modelled in the r-z plane, as indicated with *hatches*

[1] The vector equality $\nabla \times (\nabla \times \mathbf{A}) = \nabla(\nabla \cdot \mathbf{A}) - \nabla^2\mathbf{A}$ is applied.

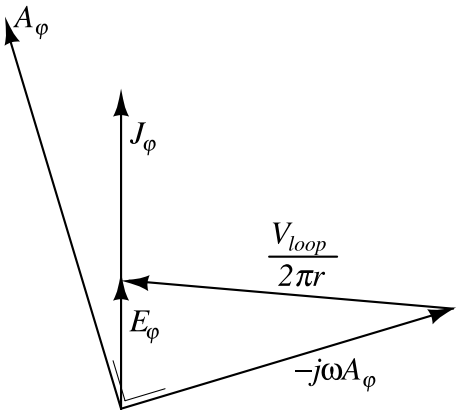

Fig. 2.7 Phasor diagram of the scalar variables of an axisymmetric FE model according to (2.46)

In other words, $\frac{J_\varphi^e}{\sigma}$ fulfils the same role as $-\nabla V$ in (2.42). In this way, the axisymmetric limitation of not allowing a conservative field in the φ direction is circumvented. Equivalent to an external current density J_φ^e, a loop voltage V_{loop} can be specified. The relation between both is:

$$J_\varphi^e = \frac{\sigma V_{loop}}{2\pi r} \tag{2.47}$$

Equation (2.46) is graphically represented by means of a phasor diagram in Fig. 2.7. It sketches the relative position of phasors A_φ, E_φ, J_φ and V_{loop} in the complex plane.

Integration of (2.45) over an axisymmetric contour C with radius r yields:

$$V_{loop} = 2\pi r j\omega A_\varphi + 2\pi r \frac{J_\varphi}{\sigma} \tag{2.48}$$

Simplifying the first term of this equation and introducing the infinitesimal surface $\mathrm{d}S$ in the second term, one obtains:

$$V_{loop} = j\omega\phi + \frac{2\pi r}{\sigma\,\mathrm{d}S}\,\mathrm{d}I_\varphi \tag{2.49}$$

The second term can be recognised as the DC ohmic resistance of a conductor times the current through it (Ohm's law). When ω is zero, this term on its own governs the current-voltage relation. It can be calculated for each contour C independently and is proportional to the length $2\pi r$. The first term in (2.49) cannot be calculated independently for each contour, as the flux ϕ enclosed by C is a result of the total current carried by the inductor. In general, A_φ and hence ϕ are not constant over the wire or winding cross-section. Therefore, for a constant V_{loop} over the wire cross-section, the second term in (2.49) has to compensate for variations of the first term. The consequence is a heterogeneous current distribution, with varying phase, over the wire cross-section [12].

For an individual wire, current tends to concentrate along the outer wall, hence the name skin effect. For the influence of the current through neighbouring wires,

the term proximity effect applies. A useful parameter for assessing the degree to which skin and proximity effect take place, is the skin depth δ [69]. It is defined as the distance over which an EM planar wave in a conductive medium is attenuated by $1/e$ (≈ 0.37):

$$\delta = \sqrt{\frac{2}{\omega\mu\sigma}} \tag{2.50}$$

By rule of thumb, the effect on the AC resistance becomes noticeable when the skin depth is smaller than the diameter of the wire. For copper for example, the skin depth at 1 MHz is 65 μm.

2.5.1.1 DC Models

Although in reality AC signals are generally applied over an inductor, a DC model may be sufficient to calculate the inductance of a coil winding. This approximation implies that current redistribution over the wire cross-section does not noticeably influence the inductance value. This true for most practical coils, with dimensions normally much larger than the diameter of the wire.

In the DC case, (2.44) further simplifies to:

$$-\frac{1}{\mu}\nabla^2 A_\varphi = J_\varphi^e \tag{2.51}$$

Some examples of DC, axisymmetric finite element models are given next.

Example 1 (Inductance of a solenoid) Figure 2.8 depicts a DC axisymmetric model of a solenoid. The black rectangle represents the winding cross-section of the solenoid. In reality consisting out of multiple turns, a more or less homogeneous current distribution can be assumed over this cross-section. Hence, a constant current density J_φ^e has been applied over it. The shading indicates the calculated vector potential A_φ. The resulting magnetic field lines are plotted in white.

Using the vector potential definition (2.15) and Stokes's theorem, the magnetic flux enclosed by the circular contour at (r, z) is:

$$\phi\,(r, z) = 2\pi r\, A_\varphi\,(r, z) \tag{2.52}$$

As A_φ is not constant over the winding cross-section, the calculated flux ϕ depends on the particular contour followed. Yet ϕ, L and M in (2.27) and (2.28) are well-defined. To resolve this ambiguity, one has to consider that in reality the winding cross-section consists out of multiple turns. The inhomogeneity of the vector potential A_φ hence corresponds to a difference in emf over the different turns. The average emf is obtained by taking the average magnetic flux:

$$\overline{\phi} = \frac{1}{S}\iint_S 2\pi r\, A_\varphi \,\mathrm{d}r\,\mathrm{d}z \tag{2.53}$$

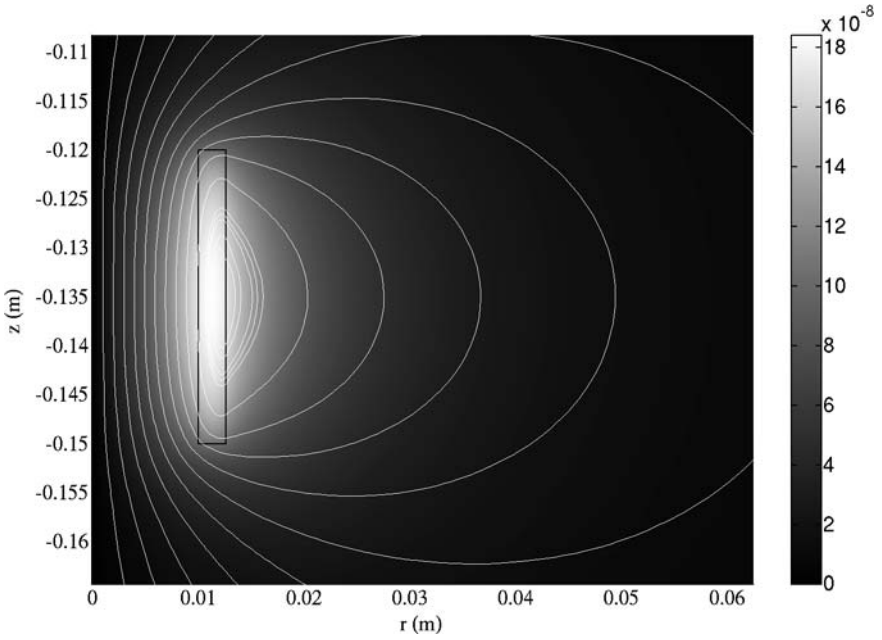

Fig. 2.8 DC axisymmetric FE model of a solenoid. The *z-axis* is the axis of rotational symmetry, the rectangle represents the winding cross-section of the solenoid. The vector potential A_φ (*shading*, in units of Tm) and the magnetic field (*stream lines*) are plotted

where S is the area of the winding cross-section. The inductance of the solenoid is then calculated as:

$$L = \frac{N^2 \overline{\phi}}{\iint_S J_\varphi^e \, \mathrm{d}r \, \mathrm{d}z} \tag{2.54}$$

where N is the number of turns. One factor of N sums the voltages of all individual turns. The other factor of N accounts for the fact that each more turn causes a proportionally higher current density J_φ^e for the same amount of current fed into the coil.

A DC model like this is only as accurate as the modelled current distribution matches the real distribution at the frequency of interest. For the example in Fig. 2.8, L is calculated to be $11.4N^2$ nH.

Example 2 (Inductance of a planar, spiral coil) Figure 2.9 depicts a FE model for a spiral inductor, completely analogous to the previous model. Here each turn is modelled separately, but again with a homogeneous current distribution. The calculated inductance L is 730 nH.

For the models developed above, air is used as the only surrounding medium. Magnetic materials like ferrite cores however are easily included in this kind of FE models.

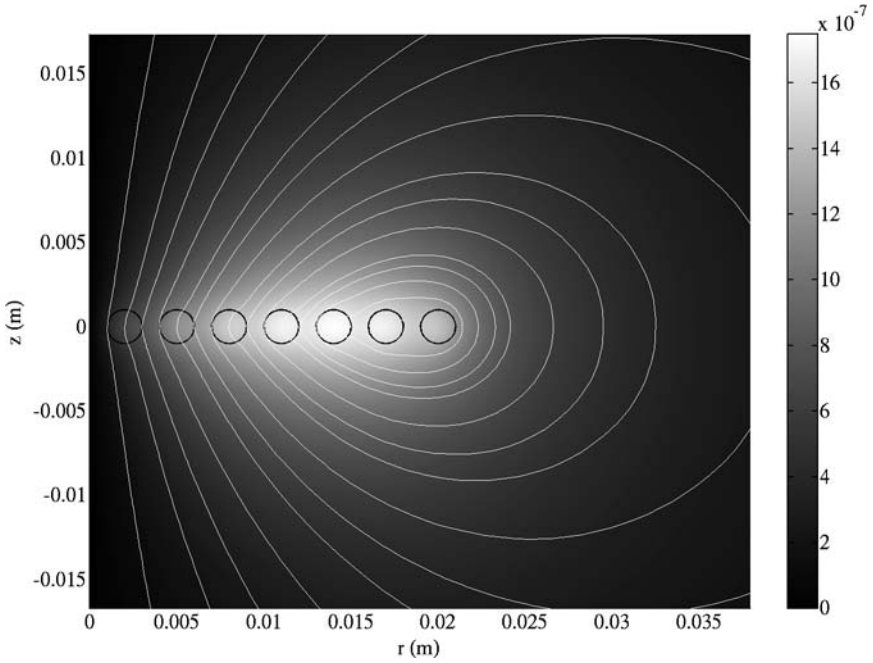

Fig. 2.9 DC axisymmetric FE model of a spiral coil. The *circles* represent the seven individual turns. The vector potential A_φ (*shading*, in units of Tm) and the magnetic field (*stream lines*) are plotted

2.5.1.2 AC Models

To calculate the real current distribution instead of assuming it to be known, an AC analysis is mandatory. Equation (2.44) is to be solved for each strand in the winding cross-section of a coil. Apart from the inductance, also the AC equivalent series resistance (ESR) can then be calculated. This is demonstrated in the next few examples.

Example 3 (Inductance and ESR of a three-winding solenoid) In Fig. 2.10, an axisymmetric FE model of a small solenoid is solved at a frequency of 1 MHz. A different V_{loop} across each of the copper turns is allowed, while the current is enforced to be equal through all. To meet this latter condition, the solver iterates over the V_{loop} values until an acceptable solution is found. The resulting current distribution over the wire cross-sections is plotted in Fig. 2.10 together with the magnetic field lines. One clearly observes the proximity effect here. Both the inductance L and the ESR R of the solenoid can now be found from:

$$\frac{V_{loop1} + V_{loop2} + V_{loop3}}{I} = j\omega L + R \tag{2.55}$$

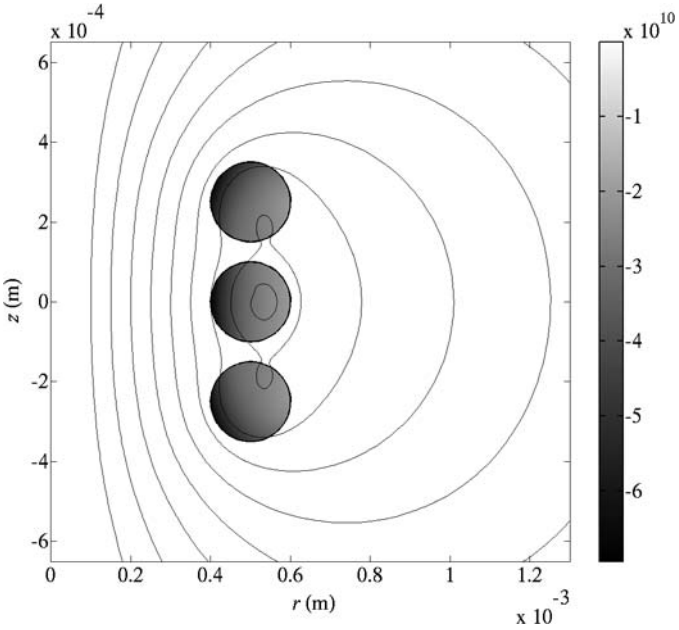

Fig. 2.10 AC axisymmetric FE model of a small solenoid. The three *circles* represent the three copper turns. The current density amplitude $|J_\varphi|$ in each strand is shown in units of A/m^2 (*shading*) at a frequency of 1 MHz. The *stream lines* of the magnetic field are plotted in *black*

where the current I is the integration of the current density over any of the wire cross-sections, S_1 for instance:

$$I = \iint_{S1} J_\varphi \, \mathrm{d}r \, \mathrm{d}z \tag{2.56}$$

For the solenoid in Fig. 2.10, the following result are obtained:

$$L = 6.1 \text{ nH} \tag{2.57}$$

$$R = 9.7 \text{ m}\Omega \tag{2.58}$$

Example 4 (Inductance and ESR of an infinitely long solenoid) FE models for structures that exhibit a certain degree of symmetry or periodicity can usually be reduced in size by applying the appropriate boundary conditions.

Figure 2.11 shows an axisymmetric AC model for a long solenoid composed of two layers of turns. Only one elementary part of the solenoid is solved for, but in fact it is an infinitely long solenoid that is modelled. Along the upper and lower boundaries $z = 0$ and $z = 55$ µm, the tangential component of the magnetic field is set to zero:

$$\hat{\mathbf{n}} \times \mathbf{H} = 0 \tag{2.59}$$

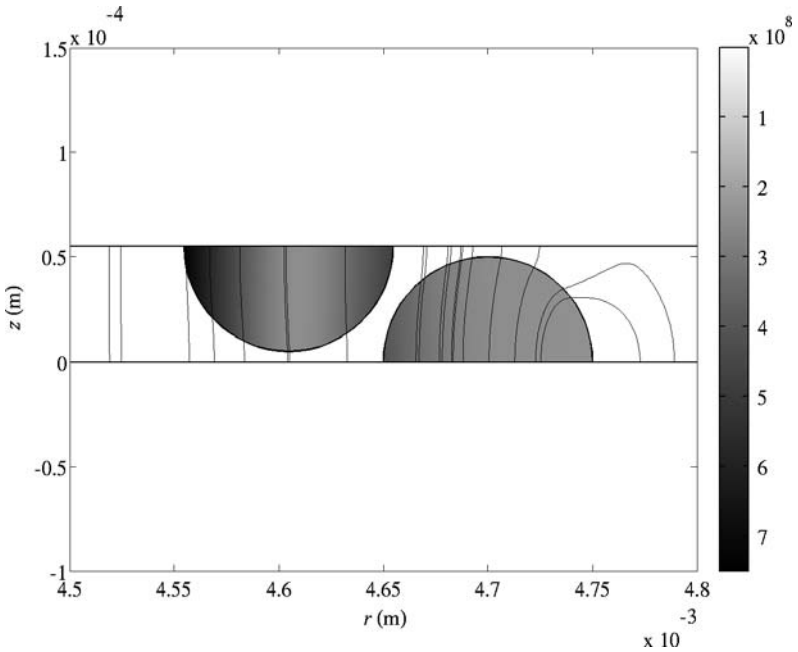

Fig. 2.11 AC axisymmetric FE model for an infinitely long solenoid. The winding consists of two layers of 100 µm copper wire with 5 µm insulation thickness. The turns are at closest distance. The current density amplitude $|J_\varphi|$ in each strand is shown in units of A/m^2 (*shading*) at a frequency of 1 MHz. The *stream lines* of the magnetic field are plotted in *black*

with $\hat{\mathbf{n}}$ the unity vector perpendicular to the boundary. This condition ensures symmetry across both boundaries and in this way assumes an infinitely long solenoid. The boundary at $r = 0$ (not shown) remains the axis of revolution and the boundary at $r = 5$ cm still is that of magnetic isolation:

$$A_\varphi = 0 \tag{2.60}$$

Again, an equal current is forced through both turn halves. The resulting current distribution is shown in Fig. 2.11 together with the magnetic field. The L and R values can again be calculated from (2.55). For the example in Fig. 2.11 at a frequency of 1 MHz, one ends up with:

$$L = 1.5N\ \mu\text{H} \tag{2.61}$$

$$R = 114N\ \text{m}\Omega \tag{2.62}$$

Note that this time only a single factor of N appears because each additional turn implies a longer solenoid. The validity of these results depends on the length of the actual coil. The calculated inductance L usually is not a good match to the real one, due to the unrealistic uniformity of the vector potential along the length of the solenoid (compare with Fig. 2.8). Full-geometry DC models, like the one in Fig. 2.8, are better suited to calculate inductance values.

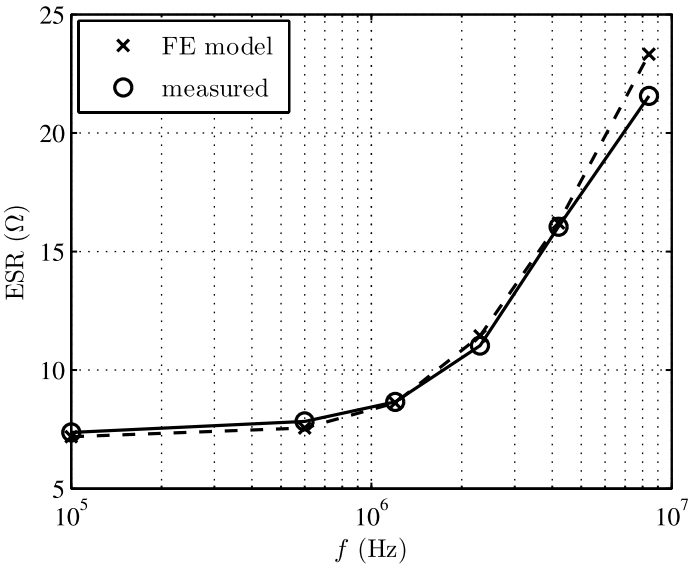

Fig. 2.12 Calculated and measured ESR of a single-layer solenoid winding vs. frequency f. The inner coil diameter is 9.2 mm, the copper wire diameter is 100 µm and the 115 turns lay equally spread over a length of 13.8 mm

The calculated R on the other hand, is in good agreement with reality. To demonstrate this, the equivalent series resistance of a single-layer winding is calculated and measured (Fig. 2.12). A single-layer winding is easier to produce in a regular way than multiple-layered structures and is hence better suited for comparison with the regular FE model. The resistance of the test coil is measured at different frequencies with an LCR meter (Appendix). Self-resonance of the test coil is observed around 10 MHz. To account for this, the corrective equations (A.3) and (A.4) are used to calculate the actual L and R values from the measured L' and R'. One can see that the R values obtained this way, match the calculations very well, even though only one turn is actually solved in the model. The apparently larger error around 8 MHz is explained by the incorrectness of Eqs. (A.3) and (A.4) close to self-resonance.

In the end, the match between the true and the modelled winding pattern determines the correctness of the calculated R value. By rule of thumb, a less regular winding results in an increased ESR for an equal coil length. The calculated ESR can therefore be regarded as some kind of minimal value for a certain coil length, wire diameter and number of turns N.

2.5.2 2-D Wire Models

Conductor cross-sections can be modelled in a 2-D geometry. Infinitely long conductors perpendicular to this plane are then assumed. An equation similar to (2.44)

is used to calculate the vector potential A_z:

$$-\frac{1}{\mu}\nabla^2 A_z + \left(j\omega\sigma - \omega^2\epsilon\right) A_z = J_z^e \tag{2.63}$$

The only difference is that Cartesian coordinates are used now, rather than cylindrical ones as in the axisymmetric case. The external current density J_z^e can be substituted by an external voltage ΔV and a conductor length l in the z-direction:

$$J_z^e = \frac{\sigma \Delta V}{l} \tag{2.64}$$

Example 5 (Partial inductance and ESR of a bond wire) The partial inductance of a piece of wire is defined as the inductance per unit length of an infinitely long wire, or equivalently, an infinite loop. In this case, there is no influence from neighbouring return currents affecting the magnetic flux around the wire. The self-inductance of a piece of wire always differs from its partial inductance. This difference is due to the mutual inductance with other pieces of the current loop (see Sect. 2.3 on page 18). These mutual inductances may be adding to the partial inductance positively or negatively.

A bond wire often makes out the largest impedance of the loop it is part of. This is true when it is longer and/or narrower than the current's return path. Where current is forced through a narrow path, the magnetic field and consequently the induced electric field $-j\omega\mathbf{A}$ are stronger, giving rise to a higher impedance than elsewhere in the loop. The total loop inductance is therefore sometimes estimated as the partial inductance of the bond wire.

Figure 2.13 depicts a 2-D FE model of an infinite, golden bond wire with a diameter of 25 µm. The current distribution is plotted for a frequency of 1 GHz. The skin depth δ is 2.4 µm at this frequency and the skin effect is total. The partial inductance L and the resistance R are calculated to be:

$$L = 1.37\ \mu\text{H/m} \tag{2.65}$$

$$R = 131\ \Omega\text{/m} \tag{2.66}$$

2.5.3 3-D Models

Some structures can only be modelled in a fully three-dimensional geometry. As far as the static (DC) case is concerned, 3-D modelling is generally feasible with a FE package. AC analysis of 3-D geometries on the other hand is far from straightforward and usually requires a deeper understanding of the subject of FE modelling. Therefore, 3-D AC modelling is not considered here, neither has it been used in the research presented by this text.

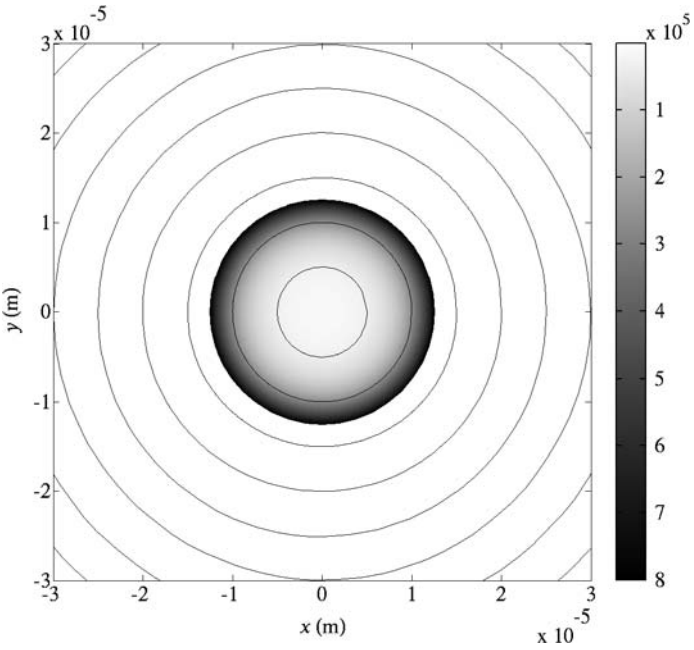

Fig. 2.13 2-D AC FE model of a golden bond wire of 25 μm diameter. The current density amplitude $|J_z|$ is plotted in *shades of grey* and in units of A/m^2 at a frequency of 1 GHz. The *black concentric circles* are the magnetic field lines

In the static case, (2.40) and (2.41) become:

$$\nabla \times \left(\mu^{-1} \nabla \times \mathbf{A}\right) = -\sigma \nabla V + \mathbf{J^e} \tag{2.67}$$

$$\nabla \cdot \left(\sigma \nabla V - \mathbf{J^e}\right) = 0 \tag{2.68}$$

These equations can be solved independently. The total current density $-\sigma \nabla V + \mathbf{J^e}$ is first found from the applied potentials and external current densities through (2.68). This result is then used as an input for equation (2.67) to find the magnetic potential and fields.

Example 6 (Inductance of a square Helmholtz coil) A Helmholtz coil encompasses two identical coils placed parallel to each other, separated by a distance usually more or less equal to the outer coil dimension.

In this example, square shaped coils are employed with an inner dimension of 40 cm and a square winding cross-section of 2 cm. The distance from one coil to the other measures 44 cm. This problem can be reduced to the geometry in Fig. 2.14. Only one of the coils and one octant of 3-D space is actually modelled. The solution for the rest of the geometry follows out of symmetry. Along the boundary planes $z = 0$ and $z = 23$ cm, (2.59) applies, setting the tangential magnetic field component

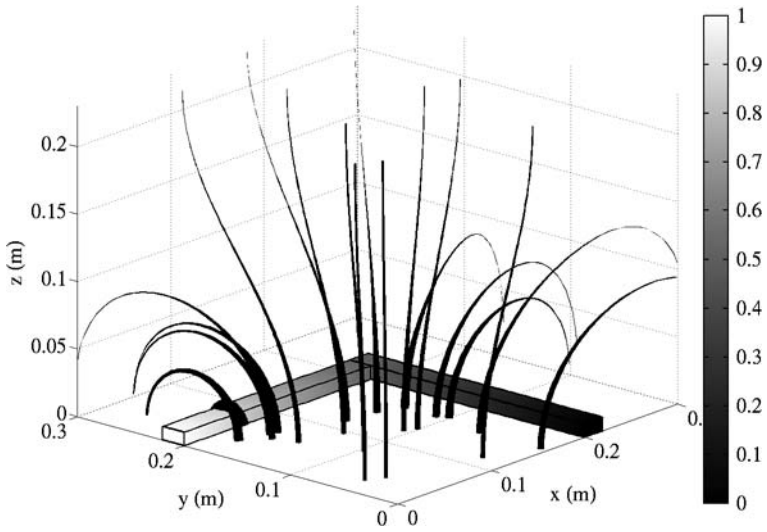

Fig. 2.14 DC FE model of a square Helmholtz coil. Only one octant of one of the coils is modelled. The voltage across the conductor is visualised by the *grey shading* (unit: V). The magnetic field lines are plotted as well: *thicker lines* indicate stronger fields

to zero. It accounts for the symmetry across both planes. The symmetry across the plane at $z = 23$ cm is due to the other coil of the Helmholtz pair, displaced by 46 cm along the z-direction. By enforcing symmetry across both planes this way, in fact an infinite stack of identical coils is modelled, much like the infinitely long solenoid of Example 4. One can hence expect the calculated field to be slightly larger than the field obtained with a stack of only two coils. Along planes $x = 0$ and $y = 0$, the tangential component of the magnetic potential is set to zero:

$$\hat{\mathbf{n}} \times \mathbf{A} = 0 \tag{2.69}$$

As a result, the magnetic flux density $\mathbf{B}$ is tangential to the planes $x = 0$ and $y = 0$. Hence, symmetry is obtained with the other quadrants across these vertical mirror planes. The other boundary planes of the model follow the same boundary condition (2.69) and are put away far enough from the origin to simulate an infinite space.

Because it is hard to define an external current density $\mathbf{J}^{\mathbf{e}}$ in this 3-D model, a voltage is applied at the terminals of the quarter coil. The resulting potential V is shown in Fig. 2.14 along the conductor boundaries in shades of grey. In a next step, the current density $-\sigma \nabla V$ is used to calculate the magnetic field, also plotted.

The inductance can again be calculated by integration and averaging of the vector potential A over the conductor. A more convenient alternative however is the integration of the magnetic energy density $w_m = \frac{\mathbf{B} \cdot \mathbf{H}}{2}$ over the complete space. Here, this integral is simplified to 16 times the integral over the modelled volume V_{mod}:

$$\frac{LI^2}{2} = 16N^2 \int_{V_{mod}} w_m \, \mathrm{d}V \tag{2.70}$$

with N the number of turns of one coil. The factor N^2 arises, as always, from the fact that I is divided by N to have an equal global current distribution and that the induced emf is perceived over N turns in series. For the Helmholtz coil in Fig. 2.14, a total inductance $L = 2.3N^2$ µH is calculated when both coils are connected in series and $L = 575N^2$ nH when they are connected in parallel.

2.5.4 Mutual Inductance

Thus far the developed FE models have been used to calculate self-inductance and where appropriate the equivalent series resistance. The same FE models can be used to calculate the mutual inductance of the modelled inductor with an arbitrary secondary coil. Like for the self-inductance, usually a DC model suffices to calculate mutual inductances.

Once the magnetic field induced by a certain source current is known, the mutual inductance can be calculated by simply integrating the magnetic flux density over the surface of interest (Eq. (2.28)). This may involve exporting the FE solution to more advanced numerical computation packages, like MATLAB [149]. Integration over surfaces that do not conform to the symmetry of the original model, can also be conducted this way. Alternatively the vector potential can be integrated over a certain contour (Eq. (2.22)). For a secondary coil with a certain winding thickness, the calculated flux should be averaged over its winding cross-section, as explained in Sect. 2.5.1.1 on page 27.

2.6 Conclusions

The electric field $\mathbf{E}$ inside of a conductor can be split up into two parts: the conservative field $-\nabla V$ corresponding to a charge distribution ρ and the non-conservative field $-j\omega\mathbf{A}$ that is magnetically induced at non-zero frequencies. This latter field can be self-induced, i.e. the current through the conductor itself is responsible for it, or it can be induced by an external current flow. In the former case, the self-inductance L relates the magnetically induced emf across a piece of conductor with the current through it. In the latter case, it is the mutual inductance M that relates the generated emf to the external current distribution.

The current density $\sigma\mathbf{E}$ in general is heterogeneously distributed over a conductor's cross-section as $-j\omega\mathbf{A}$ is heterogeneous. The heterogeneity of $\sigma\mathbf{E}$ rises with the frequency and as a result, since the current is pushed through smaller effective areas, the losses increase as well. This reflects in a higher equivalent series resistance (ESR) of the inductive element. In principle, also the inductance values are affected by this current redistribution. For typical wire-wound coils used in inductive powering applications however, the effect on the inductance is negligible.

The capacitance distribution between the different turns of a coil determines its behaviour at higher frequencies. Since an inductive link is normally operated well

below the self-resonance frequencies of the coils, a simple RL is usually sufficient. An RLC model can be used to account for self-resonance effects. In both cases, the R value is frequency dependent.

Finite element modelling is a convenient way to calculate the self-inductance and equivalent series resistance of a coil and its coupling with other coils. To calculate self- and mutual inductances, a simple DC model with only the outer geometry of the windings and possibly that of ferromagnetic objects, is sufficient. The self- and mutual inductance are assumed not to be frequency dependent. Even three-dimensional structures are relatively easily modelled and solved at DC. To calculate the ESR on the other hand, a full AC analysis and a complete geometric definition of each turn of the winding are requisite. Symmetry and periodicity in the winding geometry can be exploited to significantly reduce the numerical size of a problem.

http://www.springer.com/978-1-4020-9074-5

Omnidirectional Inductive Powering for Biomedical Implants

Lenaerts, B.; Puers, R.

2009, XVI, 222 p., Hardcover
ISBN: 978-1-4020-9074-5